

Determining the parameters of the spiral arms of the Galaxy from kinematic tracers based on *Gaia* DR3 data

S. I. Denyshchenko,¹^{*} P. N. Fedorov,¹[†] V. S. Akhmetov,^{1,2}[‡] A. B. Velichko^{1,3} and A. M. Dmytrenko¹

¹*Institute of astronomy of V. N. Karazin Kharkiv national university, Svobody sq. 4, 61022, Kharkiv, Ukraine*

²*INAF-Osservatorio Astrofisico di Torino, Via Osservatorio 20, Pino Torinese, Turin, I-10025, Italy*

³*Department of Astronomy, University of Geneva, Chemin Pegasi 51, 1290 Versoix, Switzerland*

Accepted XXX. Received YYY; in original form ZZZ

ABSTRACT

We present the results of determining the parameters of the spiral arms of the Galaxy using the stars *Gaia* DR3, whose absolute magnitude is $M_G < 4$, and which allow tracing spiral arms at large distances from the Sun. As tracers of spiral arms, we use the centroids of stellar spherical regions with a radius of 0.5 kpc, in which the deformation velocities along the coordinate axis R are insignificant. These kinematic tracers cover the Galactic plane within the Galactocentric coordinate ranges $140^\circ < \theta < 220^\circ$ and $4 \text{ kpc} < R < 14 \text{ kpc}$. The numerical values of the pitch angles of the spirals and their Galactocentric distances to the point of intersection of the spiral with the direction of the Galactic center - the Sun are in good agreement with the results of other authors. By extrapolating beyond the data we have, we present a schematic four-arm global pattern, consisting of the Scutum–Centaurus, Sagittarius–Carina, Perseus, Norma–Outer arms, as well as the local arm Orion. The uncertainties of the determined spiral parameters confirm that the structures identified are not false, but are reliable from the statistical point of view.

Key words: methods: data analysis – Galaxy: structure – Galaxy: kinematics and dynamics – stars: kinematics and dynamics

1 INTRODUCTION

The nature of the formation of the spiral structure of the galaxy is still not determined. There are many assumptions about the causes of arms and spiral patterns in the Galaxy (Toomre 1981; Sellwood & Binney 2002; Masset & Tagger 1997; Merrifield et al. 2006; Patsis 2006; Quillen et al. 2011)

According to the classical wave theory, proposed by Lin & Shu (1964), spiral arms are waves of increased density rotating around the center of the Galaxy as a solid body at a constant angular velocity (i.e., pattern velocity), despite the differential rotation of stars and interstellar medium, that results in long lifetime of spiral arms (see also Shu 2016). To date, many works have been devoted to the study of the spiral structure, using various methods and objects (Lin & Shu 1964; Lin et al. 1969; Georgelin & Georgelin 1976; Taylor & Cordes 1993; Russeil 2003; Paladini et al. 2004; Popova & Loktin 2005; Dias & Lépine 2005; Levine et al. 2006; Moitinho et al. 2006; Vázquez et al. 2008; Gerhard 2011; Efremov 2011; Bobylev & Bajkova 2014; Hou & Han 2014, 2015; Dambis et al. 2015; Reid et al. 2019; Xu et al. 2018, 2021; Poggio et al. 2021; Hao et al. 2021). Most of these methods are based on the analysis of trigonometric parallaxes and radial velocities of young objects such as OB stars, open clusters, hydrogen clouds, HII regions, giant molecular clouds, methanol masers, etc. However, the spiral structures of the Galaxy contain not only young objects, but also most other types of objects, including red giants and subgiants. For example, Junqueira et al. (2015) used a

sample of giants of different ages for a new method for determining the velocity of the Milky Way spiral pattern based on the interaction between spiral arms and disk stars. The main problems in the studies given above are the difficulty in determining trigonometric parallaxes, their significant errors, as well as the limited number of samples of the objects under study.

The third release of the *Gaia* space mission, which contains high-precision proper motions, parallaxes, radial velocities and other astrometric and astrophysical parameters for stars of various types, makes it possible to analyze in great details the structural features of an extended region of our Galaxy. A large sample of objects can be used not only to analyze the spatial structure of the Galaxy from positions of the objects, but also to perform a detailed kinematic analysis of Galactic various regions, that makes it possible to obtain additional information about the structural features of these regions. A frequently used physical model for studying stellar kinematics is the Ogorodnikov–Milne (O–M) model (Ogorodnikov 1965; Clube 1972; Du Mont 1977; Miyamoto & Soma 1993; Miyamoto & Zhu 1998). This model makes it possible to study the velocity field in a deformable stellar system. Fedorov et al. (2021, 2023) proposed a method for obtaining kinematic parameters within the framework of the O–M model for stellar systems whose centroids are located in the Galactic plane. In these works, the region of determination of the kinematic parameters of stellar systems has been extended to heliocentric distances up to 10 kpc.

One of the main goals of the spiral structure theory, which is based on observational data, is to explain the stability of spiral patterns. Why do these patterns exist throughout the many revolutions of the Galaxy, while the differential galactic rotation tends to destroy these patterns? Obviously, if the spiral pattern existed for a short

* E-mail:sofia.denyshchenko@gmail.com (SID)

† E-mail:pnfedorov@gmail.com (PNF)

‡ E-mail:akhmetovvs@gmail.com (VSA)

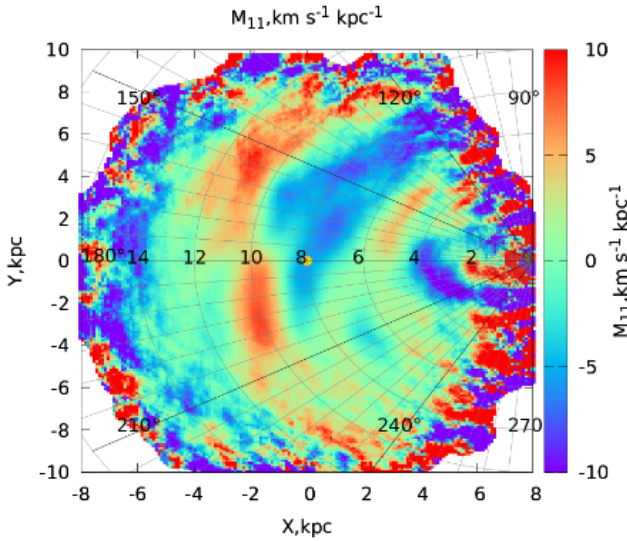


Figure 1. The O–M model parameter M_{11}^+ taken from Fedorov et al. (2023) as a function of the Galactic coordinates.

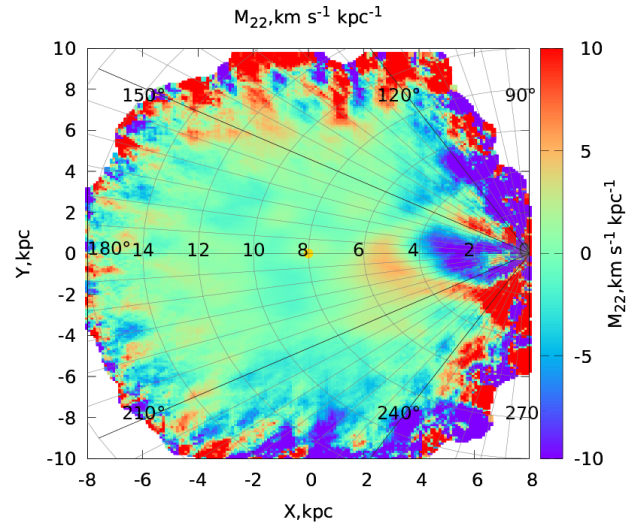


Figure 2. The O–M model parameter M_{22}^+ taken from Fedorov et al. (2023) as a function of the Galactic coordinates.

period of time, we would not observe them in a large number of disk galaxies, since differential rotation deforms any structure in the disk, causing it to be destroyed during one or two rotations of the disk. One of the possible explanations for the stability of spiral patterns is the absence of contraction-expansion deformations that destroy their shape in those regions of the Galaxy where spiral arms are located.

From a kinematic point of view, this means that in the field of stellar velocities described by the O–M model, the diagonal components of the deformation velocity tensor should be close to zero. In this case, the deformation velocities of the stellar system along the coordinate axes (relative contraction-expansion velocities) will be small on average or will be completely absent, which probably affects the stability of the stellar structure configuration. The results of determining the parameters of spiral arms given in this work are based on the assumptions mentioned above and are verified by comparing them with the results obtained in various works by other authors.

2 KINEMATIC PARAMETERS AND DATA USED

In our previous papers (Fedorov et al. 2021, 2023; Dmytrenko et al. 2023), the kinematic parameters of the O–M model for stellar systems contained in spherical regions of a 1 kpc radius, whose centroids are located in the Galactic plane, have been determined in local coordinate systems. The orientation of the local coordinate system with the origin at an arbitrary point of the Galactic plane corresponds to the following conditions: the x' axis is directed to the center of the Galaxy, the y' axis is in the direction of the Galaxy rotation, and the z' axis is perpendicular to the Galactic plane. As shown earlier (Dmytrenko et al. 2023), in the local coordinate system, the components M_{13}^+ and M_{23}^+ of the velocity deformation tensors for these stellar systems are close to zero over the entire range of changes in the Galactocentric cylindrical coordinates R and θ , which indicates the motion of stars, mainly in the Galactic plane. Therefore, in this work, we consider the tensor M^+ as flat, i.e., having only four components $M_{11}^+, M_{12}^+, M_{21}^+, M_{22}^+$, of which only three are independent ($M_{12}^+ = M_{21}^+$).

Figures 1, 2 show the diagonal components of the deformation

velocity tensor M_{11}^+ and M_{22}^+ , which have been obtained in our previous work (Fedorov et al. 2023). As can be seen from Fig. 2, in the range of angles θ from 210 to 150 degrees and distances R from 4 to 12 kpc, the magnitude of change in velocity V_θ along the unit vector \mathbf{j} (parameter M_{22}), that characterizes contraction - expansion along the y' axis of the local coordinate system is approximately $\pm 2.5 \text{ km s}^{-1} \text{ kpc}^{-1}$. Compared to the average velocity V_θ (about 240 km s^{-1}), this is approximately from 0.5 to 12% depending on R . At the same time, in the same region of the Galaxy, the M_{11}^+ parameter, which contraction - expansion along the x' axis of the system (or along the unit vector \mathbf{i}), reaches values of about $\pm 10 \text{ km s}^{-1} \text{ kpc}^{-1}$ inside some ring-shaped structures. Compared to the radial velocity V_R (about $\pm 10 \text{ km s}^{-1} \text{ kpc}^{-1}$), its change $\partial V_R / \partial R = M_{11}^+$ is almost 100% depending on R and is decisive in the formation of velocity field deformations. In this regard, for the region of the Galaxy under study, we neglect the influence of the velocity deformation along the y' axis of the local coordinate system on the stability of the stellar structure configuration.

Also, Fig. 1 clearly shows that next to these ring-shaped structures in the Galactic plane there are regions adjacent, inside which the gradient $\partial V_R / \partial R = M_{11}^+$ is close to zero. For example, this is a ring-shaped structure located at a Galactocentric distance of about 13 kpc. Similar structures, although less clear, can be seen at distances of about 9 kpc, 6 kpc, and 4 kpc. This means that the velocities of the deformation velocities along the R direction inside these regions are about zero, as a result of which there is no expansion or contraction of stellar systems along the R coordinate. Then in the case when its average value is very close to zero, there should be no deformations of the structures observed in these regions, and as a result, their shape should not change with time. The property of the invariability of the shape of structures containing objects with the kinematic parameter $\partial V_R / \partial R \approx 0$ allows us to assume that there is a relation between the stability of the spiral pattern in our Galaxy and the parameter $\partial V_R / \partial R \approx 0$.

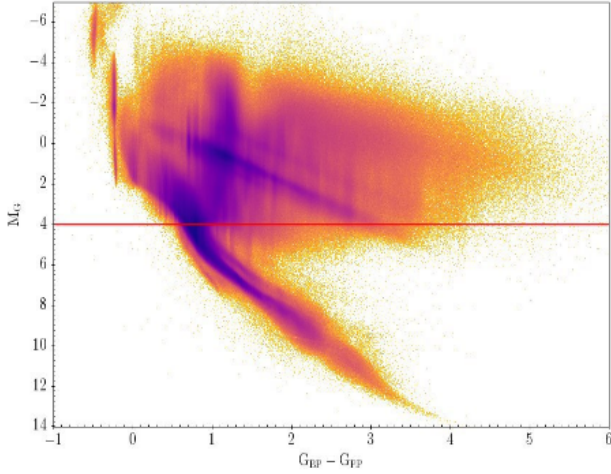


Figure 3. The color ($G_{BP} - G_{RP}$) - absolute magnitude M_G diagram based on the *Gaia* DR3 data.

2.1 Sample

To test the assumption mentioned above, we created a special sample of stars from the third release of the *Gaia* data – *Gaia* DR3 (Gaia Collaboration et al. 2016, 2023), that has been used to determine the kinematic parameters of the O–M model. The required input data of the model are positions α, δ , spatial velocities (proper motions $\mu_\alpha \cos \delta, \mu_\delta$ and radial velocities V_r) of the stars, as well as their distances (parallaxes π).

Gaia DR3 provides estimates of 5 astrometric parameters (positions, proper motions and parallaxes) for 1.8 billion stars, as well as photometry in G, G_{RP} and G_{BP} bands (Riello et al. 2021). Among them, radial velocities (the sixth astrometric parameter) have been measured for ~ 33 million objects. The presence of 6 astrometric parameters makes it possible to obtain complete information about stellar motions in space. Of these 33 million objects, we selected high-luminosity stars with absolute magnitude of $M_G < 4$ (see Fig. 3) as the base sample, see details in Akhmetov et al. (2023).

To provide the best quality of astrometric parameters, we excluded from this sample the stars for which the following conditions are satisfied:

$$\begin{cases} RUWE > 1.4, \\ \pi/\sigma_\pi < 5, \end{cases} \quad (1)$$

About 19.3 million stars meet the criteria listed above and we use them for the kinematic analysis. Since, as is known from Lindegren et al. (2021), the *Gaia* DR3 parallaxes are systematically biased relative to the expected distribution around zero by several tens of microarcseconds, we corrected them. To correct parallaxes, we used the Parallax bias Z5 computed according to Table 9 given by Lindegren et al. (2021). Our sample is limited to about magnitude 17 due to the inclusion of radial velocities. Therefore, the magnitude range of the sample has been divided into only two parts. In the range of G magnitudes from 6 to 13, we applied an offset of $-30 \mu\text{as}$, and in the range of $G > 13$, we used a value of $-40 \mu\text{as}$. Since in Fig. 20 given by Lindegren et al. (2021) jumps are observed in the range from 11.5 to 13 G magnitudes, we decided to use an average value of Z5 approximately equal to $-30 \mu\text{as}$ in this range.

In addition, we corrected for the proper motions of stars in the

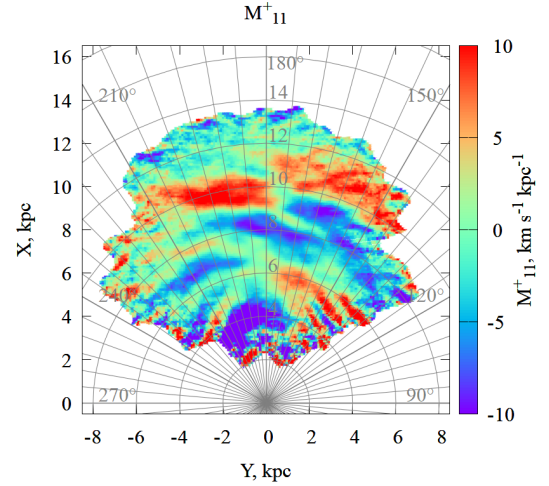


Figure 4. The O–M model parameter M_{11}^+ .

magnitude range from 6 to 13 as well. Brandt (2018); Lindegren et al. (2018) have showed that in the second release of *Gaia* (DR2) data, the reference frame of bright stars rotates relative to faint stars and quasars at a velocity of $\sim 0.15 \text{ mas yr}^{-1}$. In the early third *Gaia* release EDR3, this rotation has been previously excluded (see section 4.5 by Lindegren et al. 2021). However, an additional correction has been proposed by Cantat-Gaudin & Brandt (2021), and we use it to align the stellar proper motions in our sample brighter than $G = 13$ with the International Celestial Coordinate System.

2.2 Distribution of centroids of selected stellar systems in the Galactic plane

To solve the system of equations of the O–M model, we divided the final sample into stellar systems, which are regions inside spheres with a radius of $R_s = 0.5 \text{ kpc}$. We set the centers of these spheres at the nodes of a rectangular grid given in the Galactic plane. The grid nodes are separated from each other along the x and y coordinates at a distance of 100 pc. We chose the coverage region of the Galactic plane by the rectangular grid of nodes (centroids) within $140^\circ < \theta < 220^\circ$, $1.5 \text{ kpc} < R < 13.5 \text{ kpc}$ of Galactocentric (GC) cylindrical coordinates with distance from Sun to GC is $R_0 = 8.15 \text{ kpc}$ (see, for instance, Fig. 1, 2). We solve the system of equations of the O–M model for 12 unknowns by the least squares method (LSM) using the astrometric data of stars, the number of which in each sphere is at least 1000. Figs. 4, 5 and 6 show the dependencies of $M_{11}^+, M_{22}^+, M_{33}^+$ on the X and Y coordinates in the range of angles θ from 210 to 150 degrees and distances R from 4 to 12 kpc.

After calculating the kinematic parameters inside of each sphere, we create a subsample of centroids of those spherical regions in which the value of the parameter M_{11}^+ turned out to be insignificant, i.e. the calculated value of the parameter M_{11}^+ does not exceed twice the value of its uncertainty. As mentioned above, we do not consider the influence of the parameters M_{22}^+ and M_{33}^+ on stability, but focus only on establishing a relations between the parameters M_{11}^+ , which characterize the contraction-expansion of the velocity field in spherical regions and spiral arms. The numerical value of the radius of the spherical region equal to 0.5 kpc has been chosen from empirical considerations and is a compromise between ensuring the reliability

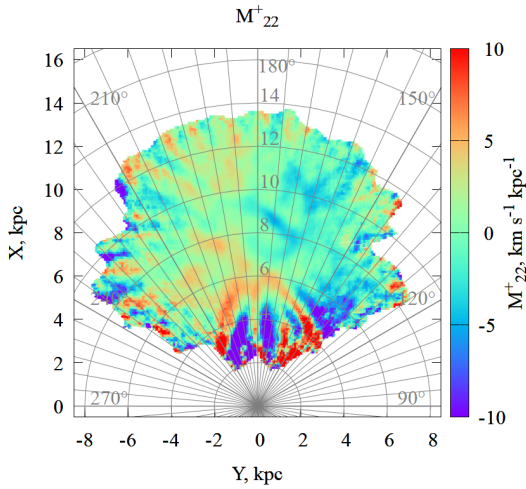


Figure 5. The O–M model parameter M_{22}^+ .

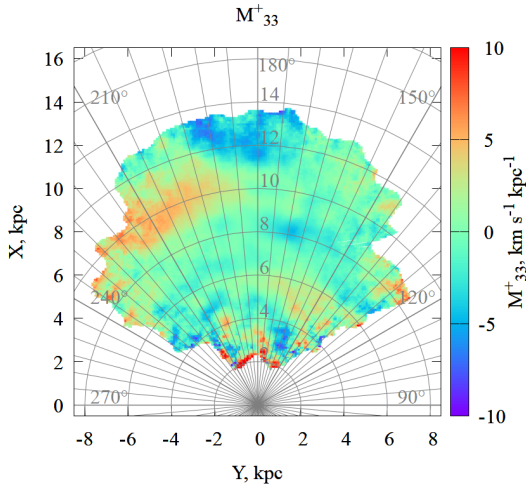


Figure 6. The O–M model parameter M_{33}^+ .

of the LSM solution (a sufficient number of stars within the sphere) and detailing of the mapped kinematic parameters.

Fig. 7 shows the distribution of the centroid coordinates in the Galactic XY plane, which are formed from stars contained in spheres with a radius of $R_s = 0.5$ kpc and having insignificant M_{11}^+ . To understand whether Fig. 7 contains the centroids belonging to some spiral arms, we superimposed the spiral arms on the centroid distribution with the parameters obtained by Reid et al. (2019), as shown in Fig. 8. As can be seen from the latter figure, individual sections of the location of the centroids on the coordinate plane are in good agreement with the superimposed spirals. In this regard, we believe that we can consider the positions of centroids with insignificant M_{11}^+ as kinematic tracers of spiral arms in the range of Galactocentric cylindrical coordinates $140^\circ < \theta < 220^\circ$, $4 \text{ kpc} < R < 13 \text{ kpc}$. The choice of these coordinate ranges is mainly due to the accuracy of the parallaxes used and the accuracy of the obtained kinematic parameters. The total number of centroids from the specified range

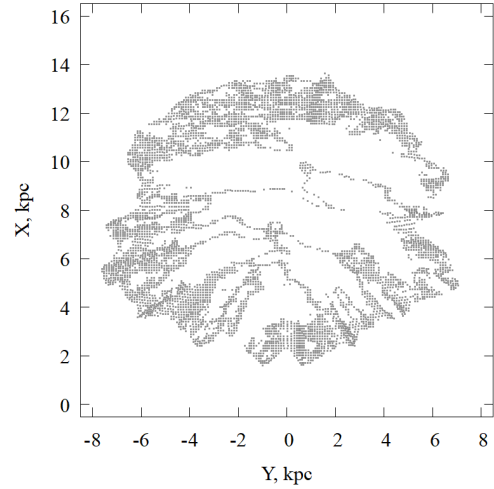


Figure 7. The distribution of the centroids coordinates in the Galactic XY plane, which are formed from stars contained in spheres with a radius of $R_s = 0.5$ kpc and having insignificant M_{11}^+ .

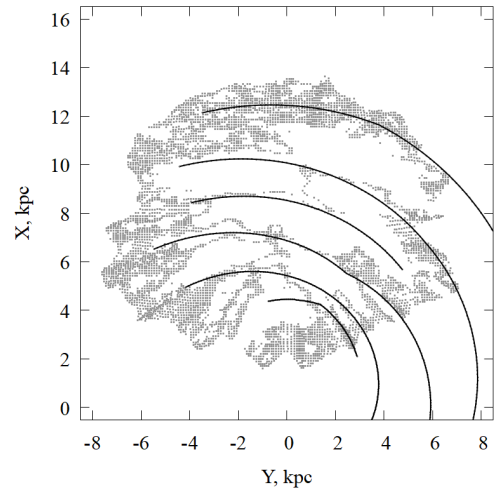


Figure 8. Same as in Fig. 7 but with superimposed spirals taken from Reid et al. (2019).

was 25,110. It is these centroids that we use further in the work as kinematic tracers of spiral arms.

3 DETERMINATION AND COMPARISON OF SPIRAL ARM PARAMETERS

To calculate the parameters of the Milky Way spirals, we apply a method that is widely used to study the spiral structure of the Galaxy from the data of various objects (Popova & Loktin 2005; Xu et al. 2013; Bobylev & Bajkova 2014; Reid et al. 2019; Hao et al. 2021; Hou 2021). The method is based on the "position angle - logarithm of the distance" diagram. Considering the centroid as a fictitious star belonging to the spiral arm, the equation that determines the position of this fictitious star on the logarithmic spiral can be written

as follows:

$$R = a_0 \exp\{(\varphi - \varphi_0) \operatorname{tg} i\} \quad (2)$$

where R is the Galactocentric distance of the centroid, $a_0 = R(\varphi = \varphi_0 = 0)$ is the Galactocentric distance to the point of intersection of the spiral with the direction of the Galactic center - the Sun, φ is the position angle of the centroid, determined from the formula $\operatorname{tg} \varphi = y/(R_0 - x)$, the value R_0 is taken equal to 8.15 kpc, x, y are heliocentric Galactic rectangular coordinates of the centroid, with the x axis directed from the Sun to the Galactic center, and the direction of the y axis coincides with that of rotation of the Galaxy; φ_0 is some arbitrarily chosen initial angle, which, for example, is taken equal to the average value of all centroid azimuths belonging to the arm. In this paper, we take the angle φ_0 equal to zero. The pitch angle of the spiral pattern is denoted as i ($i < 0$ for a leading spiral).

According to our sample, we calculate the heliocentric distance r to a particular centroid from the parallaxes corrected by us, as the average distances to stars included in each spherical region with a radius of 0.5 kpc. We calculate the Galactocentric distance R to a particular centroid and the corresponding position angle φ using the following formulas

$$R^2 = (R_0 - x)^2 + y^2 \quad (3)$$

$$\operatorname{tg} \varphi = y/(R_0 - x) \quad (4)$$

where x, y are the heliocentric Galactic rectangular coordinates of the centroid. Obviously, the relations between the position angle φ and the coordinate angle θ is $\varphi + \theta = 180^\circ$.

Since we have chosen $\varphi_0 = 0$, equation 2 can be rewritten as:

$$\ln(R/a_0) = \varphi \operatorname{tg} i \quad (5)$$

or in the form:

$$\ln(R) = \varphi \operatorname{tg} i + \ln(a_0). \quad (6)$$

The latter can be rewritten as:

$$\ln(R) = k\varphi + b \quad (7)$$

where $k = \operatorname{tg} i$, and $b = \ln(a_0)$.

As can be seen, relation 7 is the straight line equation on the plane "position angle - logarithm of distance". The solution of the system of conditional equations separately for each spiral arm by the LSM gives two quantities: k and b . Obviously, $i = \operatorname{arctg} k$, where i is the pitch angle of the spiral, and $a_0 = e^b$ and represents the Galactocentric distance of the point of intersection of the spiral with the X axis directed from the Galactic center and passing through the Sun.

The key point in the approach we use is to find those points (centroids) that belong to a particular spiral arm. Obviously, the choice of such centroids for constructing segments of straight lines on the plane "position angle φ - logarithm of the distance $\ln(R)$ " is a rather subjective procedure (see Fig. 7). We objectified the procedure for selecting points (centroids), which we use later to construct segments of straight lines, by analyzing the behavior of the centroids' radial velocities of our sample depending on the Galactocentric coordinates R and θ .

For example, Fig. 9 shows the radial velocity of the centroids of the initial sample depending on R at the fixed angle $\theta = 180^\circ$. Fig. 10 shows the same dependencies but at other coordinate angles symmetrically inclined with respect to $\theta = 180^\circ$. We built such dependencies of the radial velocities on R with a step of 1 degree in θ for the entire part of the Galaxy studied in this work. The red color on these dependencies shows the centroids for which the condition that

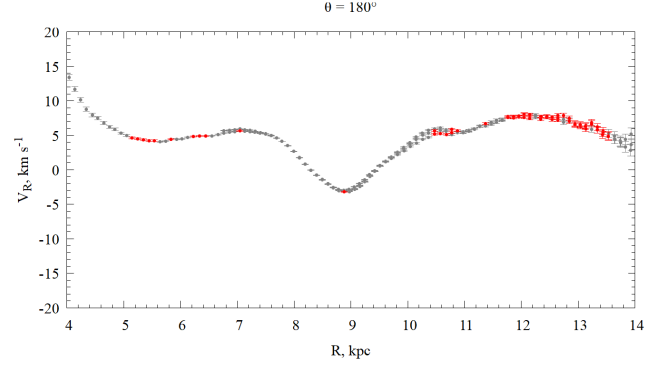


Figure 9. Dependence of the radial velocities V_R of the centroids of the original sample as a function of the Galactocentric distance R at the fixed angle $\theta = 180^\circ$. Red color shows the centroids for which the condition that the M_{11}^+ parameter is not significant has been met.

the M_{11}^+ parameter is not significant has been met. As expected, the red dots in the figures are grouped in places of local extrema, as well as in those places where the radial velocity V_R is almost constant.

It is also clearly seen from the figures that when the angle θ changes, the colored dots move along the R axis in a certain interval ΔR . In this case, the average value of the distances R_m from the intervals ΔR turned out to correlate with the Galactocentric distances to the spiral arms a_0 known from the literature. These empirical facts allowed us to form an algorithm for the selection of centroids to construct linear dependencies $\ln R = k\varphi + b$.

To form a primary list of centroids belonging to a particular arm, we use the following conditions:

1. In a spherical region with a radius of 0.5 kpc, the M_{11}^+ parameter is insignificant: $|M_{11}^+/\sigma_{M_{11}^+}| < 2$.
2. Using the method described above for first approximation values of a_0 the mean of Galactocentric distance R_m of the spiral arms turned out to be equal 5.5, 6.8, 8.76, 10.4 and 12.3 kpc for the Scutum-Centaurus arm, the Sagittarius-Carina arm, the Orion local arm, the Perseus arm and the Norma-Outer arm respectively.
3. From the analysis of various works (Dambis et al. 2015; Reid et al. 2019; Veselova & Nikiforov 2020; Hao et al. 2021; Hou 2021, and other), in the first approximation, the pitch angle of all the spiral arms i has been taken equal to -13 degrees.
4. For each spiral arm the values R_i were calculated using the above initial values of a_0 , i and position angle φ_c of the centroids by the formula 2.
5. We selected the centroids of the spherical regions with the Galactocentric distance R_c which are in the interval ± 300 pc from the value obtained in the previous step R_i for a particular spiral arm, i.e. $|R_i - R_c| < 300$ pc as we can see on Fig. 11.

We use the R_c and φ_c coordinates of centroids of spherical regions satisfying the conditions listed above to solve the equations 7 by the LSM with iterative excluding centroids according to the criterion: deviation of an individual point from the solution exceeds 2σ .

The final results of determining the parameters of the spiral arms $i = \operatorname{arctg} k$ and $a_0 = e^b$, as well as their uncertainties, are shown in Table 1 and plotted in Fig. 12.

The derived parameters of spiral arms at the level of accuracy of their determination turned out to be in good agreement with the parameters given in other studies using various tracers (see Table 2).

Below we present plots for linear dependencies on the "position angle - logarithm of distance" plane and plots of logarithmic spirals

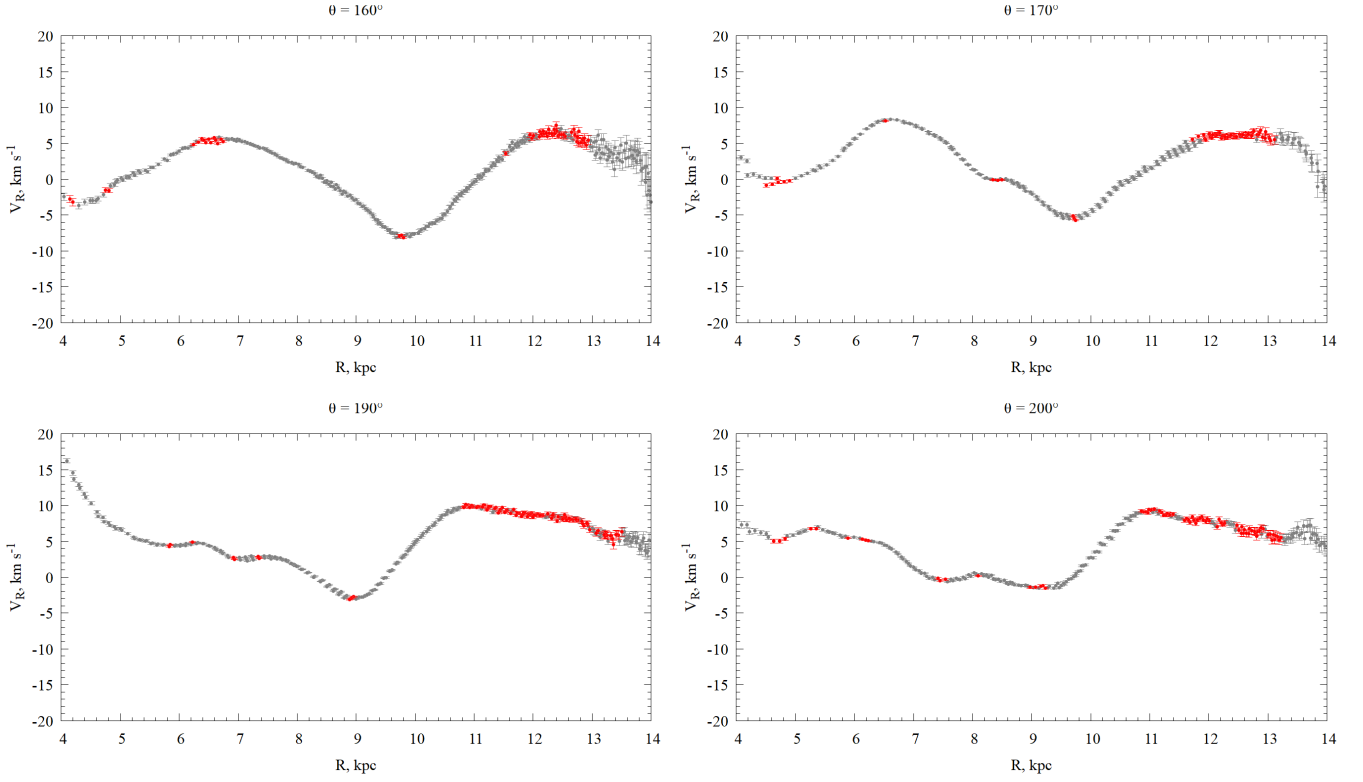


Figure 10. Same as in Fig. 9 but at other fixed coordinate angles: $\theta = 160^\circ$ (top left), 170° (top right), 190° (bottom left) and 200° (bottom right).

Table 1. Parameters of spiral arms. I - Scutum–Centaurus arm, II - Sagittarius-Carina arm, III - Perseus arm, IV - Outer arm, Local - Orion arm. N is the number of centroids used.

| | I | II | Local | III | IV |
|-------|-------------------|-------------------|-------------------|--------------------|--------------------|
| i | -12.04 ± 0.34 | -12.07 ± 0.17 | -12.43 ± 0.32 | -12.07 ± 0.18 | -12.43 ± 0.18 |
| a_0 | 5.493 ± 0.014 | 6.878 ± 0.010 | 8.719 ± 0.022 | 10.470 ± 0.012 | 12.289 ± 0.009 |
| N | 151 | 202 | 122 | 215 | 371 |

Table 2. Parameters of spiral arms. (1) - [Bobylev & Bajkova \(2014\)](#), (2) - [Reid et al. \(2019\)](#), (3) - [Veselova & Nikiforov \(2020\)](#), (4) - [Hou \(2021\)](#), (5) - [Xu et al. \(2018\)](#). I - Scutum–Centaurus arm, II - Sagittarius-Carina arm, III - Perseus arm, IV - Outer arm, Local - Orion arm.

| | I | II | Local | III | IV | Ref |
|-------|-----------------|-----------------|-----------------|-----------------|------------------|-----|
| i | -11.2 ± 4.0 | -9.3 ± 2.2 | -10.2 ± 0.3 | -14.8 ± 0.8 | -11.5 ± 1.9 | 1 |
| | -13.1 ± 2.0 | -9.0 ± 1.9 | -11.4 ± 1.9 | -9.5 ± 2.0 | -6.2 ± 4.2 | 2 |
| | -11.7 ± 0.9 | -13.1 ± 1.4 | -9.9 ± 1.2 | -6.2 ± 1.6 | -5.2 ± 2.8 | 3 |
| | -8 | -13.8 | -8.5 | -11.9 | | 4 |
| | -18.7 ± 0.8 | -13.5 ± 0.5 | -11.5 ± 0.5 | -9.0 ± 0.1 | | 5 |
| a_0 | 4.5 ± 0.2 | 6.8 ± 0.3 | 8.1 ± 0.3 | 9.9 ± 0.4 | 13.5 ± 0.5 | 1 |
| | 4.9 ± 0.1 | 6.0 ± 0.1 | 8.3 ± 0.1 | 8.9 ± 0.1 | 12.2 ± 0.4 | 2 |
| | 6.07 ± 0.04 | 6.78 ± 0.05 | 8.19 ± 0.05 | 9.74 ± 0.09 | 12.02 ± 0.17 | 3 |
| | 6.5 | 6.9 | 8.5 | 9.6 | | 4 |
| | 5.9 ± 0.1 | 7.2 ± 0.1 | 8.3 ± 0.1 | 10.6 ± 0.1 | | 5 |

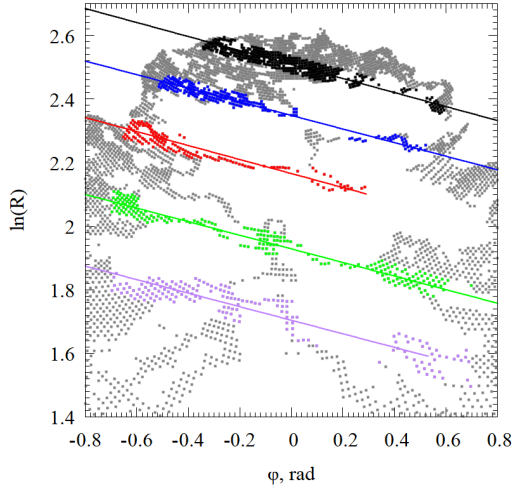


Figure 11. Dependence of $\ln(R)$ on the position angle φ . Blue dots and line (–) corresponds to the Perseus arm, green dots and line (–) to the Sagittarius-Carina arm, black dots and line (–) to the Outer arm, violet dots and line (–) to the Scutum-Centaurus arm, red dots and line (–) to the Orion local arm.

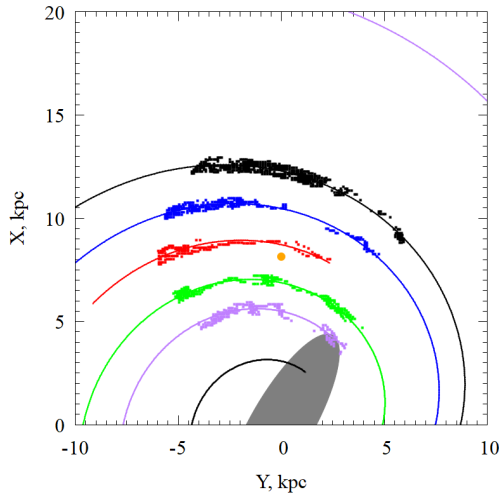


Figure 12. Logarithmic spirals plotted using the corresponding parameters derived in this work and given in Table 1. Color points show the centroids belonging to corresponding spiral arms. The gray ellipse shows the Galactic bar reproduced according to the data obtained by Wegg et al. (2015).

constructed in the Galactic plane according to the data in Table 1. Specific dependencies are color-coded. Violet color corresponds to the Scutum-Centaurus arm, green – to the Sagittarius-Carina arm, red – to the Orion local arm, blue – to the Perseus arm, and black – to the Norma-Outer arm. All figures are built according to the algorithm described above.

4 RESULTS AND DISCUSSION

Fig. 13 shows the four main spiral arms of the Milky Way in the rectangular Galactocentric coordinate system. They are built according to the parameters determined in this work by extrapolation beyond the data we have and schematically represent the spiral pattern of our

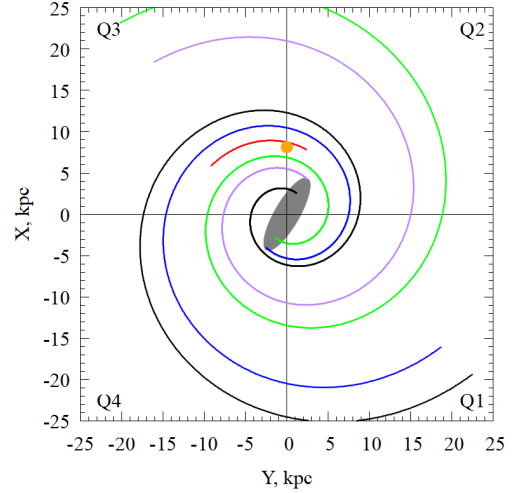


Figure 13. Schematic representation of the the spiral pattern of the Milky Way in the rectangular Galactocentric coordinate system. Blue curve (–) corresponds to the Perseus arm, green curve (–) to the Sagittarius-Carina arm, black curve (–) to the Outer arm, violet curve (–) to the Scutum-Centaurus arm, red curve (–) to the Orion local arm. The yellow point shows the position of the Sun. The gray ellipse shows the Galactic bar reproduced according to the data obtained by Wegg et al. (2015).

Galaxy (Grand design). Also, Fig. 13 shows the Galactic bar reproduced according to the data obtained by Wegg et al. (2015), where the major and minor axes of the bar were determined to be 5 and 1.5 kpc, respectively (see Rattenbury et al. 2007; Cao et al. 2013, as well). Its major axis inclination to the X-axis is approximately 30° . The bar is shown in Fig. 13 schematically as a filled gray ellipse.

Note that, unlike other works, we do not use the concept of "kink" in an arm, introduced by Reid et al. (2019), but assumed that any arm as a whole can be characterized by one value of the pitch angle of. It is also worth noting that we could not determine the width of the spiral arms in this work. However, it can be recalled that the used tracers of the spiral arms are maximally separated by 600 pc in the Galactocentric distance, which can be considered as a lower estimate of their width.

As can be seen from the figure, the spiral arms intersect with the major axis of the bar at four points. The intersection points of the Norma-Outer and Scutum-Centaurus arms with the major axis of the bar are located in the second Galactocentric quadrant Q2 and have approximate coordinates $x_N = 2.5$, $y_N = 1.0$; $x_{Sc} = 4.0$, $y_{Sc} = 2.5$ kpc, respectively. The Norma-Outer arm starts at the indicated point and continues into the quadrants Q3 and Q4, going counterclockwise into the quadrant Q1. The Scutum-Centaurus arm originates approximately near the point $x_{Sc} = 4.0$, $y_{Sc} = 2.5$ kpc in the quadrant Q2 and extends counterclockwise into the Q3 quadrant and then into the quadrant Q1.

The Sagittarius-Carina and Perseus arms start near the far end of the bar and have approximate coordinates $x_S = -3.0$, $y_S = -1.5$ kpc; $x_P = -4.0$, $y_P = -2.5$ kpc, respectively. The Sagittarius-Carina arm from the quadrant Q4 passes counterclockwise through the quadrants Q1, Q2 and Q3. The Perseus arm starts at Q4, passes through Q1, Q2 and Q3, and extends further counterclockwise.

The behavior of spiral arms described above practically coincides with the descriptions of their behavior given in various works to which we refer.

5 CONCLUSIONS

The parameters of the spiral structure obtained in this work indicate their good agreement with the results obtained by other authors using various indicators of the spiral structure and different approaches for their determination. The use in this work of statistically insignificant kinematic parameters M_{11}^+ for the selection of centroids, the positions of which are considered as kinematic tracers of spiral arms, turned out to be a fairly reliable method.

Note that although the number of centroids used to determine the spiral parameters is a few hundred, the number of stars in spherical regions reaches hundreds of thousands. This allows us to determine the kinematic parameters, as well as the positions of the centroids with high accuracy, which saves us from arbitrariness when choosing tracers for fixing specific spiral arms.

The proposed approach made it possible to find stable structures in the Galaxy, in particular, to reveal spiral arms and determine their parameters. In addition, the method used makes it possible to obtain information not only about spiral arms, but also some additional information. For example, as Figs. 7 and 11 show, stable structures (M_{11}^+ - insignificant) exist not only in the form of spirals, but also in the form of some formations extending in the space between them. The interpretation of these facts requires further accurate study, which is beyond the scope of this article.

DATA AVAILABILITY

The used catalogue data is available in a standardised format for readers via the CDS (<https://cds.u-strasbg.fr>). The software code used in this paper can be made available upon request by emailing the corresponding author.

6 ACKNOWLEDGEMENTS

This work has made use of data from the European Space Agency (ESA) mission *Gaia* (<https://www.cosmos.esa.int/gaia>), processed by the *Gaia* Data Processing and Analysis Consortium (DPAC, <https://www.cosmos.esa.int/web/gaia/dpac/consortium>). Funding for the DPAC has been provided by national institutions, in particular the institutions participating in the *Gaia* Multilateral Agreement.

We are immensely grateful to the Armed Forces of Ukraine for the fact that in wartime we still have the opportunity to work and do science.

References

Akhmetov V. S., Bucciarelli B., Crosta M., Lattanzi M. G., Spagna A., Re Fiorentin P., Bannikova E. Y., submitted in 2023, *MNRAS*,
 Bobylev V. V., Bajkova A. T., 2014, *MNRAS*, 437, 1549
 Brandt T. D., 2018, *ApJS*, 239, 31
 Cantat-Gaudin T., Brandt T. D., 2021, *A&A*, 649, A124
 Cao L., Mao S., Nataf D., Rattenbury N. J., Gould A., 2013, *MNRAS*, 434, 595
 Clube S. V. M., 1972, *MNRAS*, 159, 289
 Dambis A. K., et al., 2015, *Astronomy Letters*, 41, 489
 Dias W. S., Lépine J. R. D., 2005, *ApJ*, 629, 825
 Dmytrenko A. M., Fedorov P. N., Akhmetov V. S., Velichko A. B., Denyshchenko S. I., 2023, *MNRAS*, 521, 4247
 Du Mont B., 1977, *A&A*, 61, 127
 Efremov Y. N., 2011, *Astronomy Reports*, 55, 108

Fedorov P. N., Akhmetov V. S., Velichko A. B., Dmytrenko A. M., Denyshchenko S. I., 2021, *MNRAS*, 508, 3055
 Fedorov P. N., Akhmetov V. S., Velichko A. B., Dmytrenko A. M., Denyshchenko S. I., 2023, *MNRAS*, 518, 2761
 Gaia Collaboration et al., 2016, *A&A*, 595, A1
 Gaia Collaboration et al., 2023, *A&A*, 674, A1
 Georgelin Y. M., Georgelin Y. P., 1976, *A&A*, 49, 57
 Gerhard O., 2011, *Memorie della Societa Astronomica Italiana Supplementi*, 18, 185
 Hao C. J., et al., 2021, *A&A*, 652, A102
 Hou L. G., 2021, *Frontiers in Astronomy and Space Sciences*, 8, 103
 Hou L. G., Han J. L., 2014, *A&A*, 569, A125
 Hou L. G., Han J. L., 2015, *MNRAS*, 454, 626
 Junqueira T. C., Chiappini C., Lépine J. R. D., Minchev I., Santiago B. X., 2015, *MNRAS*, 449, 2336
 Levine E. S., Blitz L., Heiles C., 2006, *Science*, 312, 1773
 Lin C. C., Shu F. H., 1964, *ApJ*, 140, 646
 Lin C. C., Yuan C., Shu F. H., 1969, *ApJ*, 155, 721
 Lindegren L., et al., 2018, *A&A*, 616, A2
 Lindegren L., et al., 2021, *A&A*, 649, A4
 Masset F., Tagger M., 1997, *A&A*, 322, 442
 Merrifield M. R., Rand R. J., Meidt S. E., 2006, *MNRAS*, 366, L17
 Miyamoto M., Soma M., 1993, *AJ*, 105, 691
 Miyamoto M., Zhu Z., 1998, *AJ*, 115, 1483
 Moitinho A., Vázquez R. A., Carraro G., Baume G., Giorgi E. E., Lyra W., 2006, *MNRAS*, 368, L77
 Ogorodnikov K. F., 1965, Dynamics of stellar systems
 Paladini R., Davies R., De Zotti G., 2004, *Ap&SS*, 289, 363
 Patsis P. A., 2006, *MNRAS*, 369, L56
 Poggio E., et al., 2021, *A&A*, 651, A104
 Popova M. E., Loktin A. V., 2005, *Astronomy Letters*, 31, 171
 Quillen A. C., Dougherty J., Bagley M. B., Minchev I., Comparella J., 2011, *MNRAS*, 417, 762
 Rattenbury N. J., Mao S., Sumi T., Smith M. C., 2007, *MNRAS*, 378, 1064
 Reid M. J., et al., 2019, *ApJ*, 885, 131
 Riello M., et al., 2021, *A&A*, 649, A3
 Russeil D., 2003, *A&A*, 397, 133
 Sellwood J. A., Binney J. J., 2002, *MNRAS*, 336, 785
 Shu F. H., 2016, *ARA&A*, 54, 667
 Taylor J. H., Cordes J. M., 1993, *ApJ*, 411, 674
 Toomre A., 1981, in Fall S. M., Lynden-Bell D., eds, Structure and Evolution of Normal Galaxies. pp 111–136
 Vázquez R. A., May J., Carraro G., Bronfman L., Moitinho A., Baume G., 2008, *ApJ*, 672, 930
 Veselova A. V., Nikiforov I., 2020, *Research in Astronomy and Astrophysics*, 20, 209
 Wegg C., Gerhard O., Portail M., 2015, *MNRAS*, 450, 4050
 Xu Y., et al., 2013, *ApJ*, 769, 15
 Xu Y., Hou L.-G., Wu Y.-W., 2018, *Research in Astronomy and Astrophysics*, 18, 146
 Xu Y., Hou L. G., Bian S. B., Hao C. J., Liu D. J., Li J. J., Li Y. J., 2021, *A&A*, 645, L8